Magnetic field induced phase transitions and phase diagrams of multiferroic $Mn\_0.95Co\_0.05WO\_4$ with cycloidal spin structure

I. Urcelay-Olabarria, E. Ressouche, Z. Wang, Y. Skourski, V. Ivanov, Y. Popov, G. Vorobev, A. Balbashov, N. Qureshi, J. García-Muñoz, et al.

Magnetic field induced phase transitions and phase diagrams of multiferroic $Mn_{0.95}Co_{0.05}WO_4$ with cycloidal spin structure

I. Urcelay-Olabarria,[1,*] E. Ressouche,[2] Z. Wang,[3,4] Y. Skourski,[3] V. Yu. Ivanov,[5] Y. F. Popov,[6] G. P. Vorobev,[6] A. M. Balbashov,[7] N. Qureshi,[8] J. L. García-Muñoz,[9] V. Skumryev,[10,11] and A. A. Mukhin[5]

[1]*Departamento de Física Aplicada I, Escuela de Ingeniería de Bilbao, Universidad del País Vasco, UPV/EHU, 48013 Bilbao, Spain*

[2]*Université Grenoble Alpes, CEA, INAC, MEM, F-38000 Grenoble, France*

[3]*Hochfeld-Magnetlabor Dresden (HLD-EMFL) Helmholtz-Zentrum Dresden-Rossendorf, D-01314 Dresden, Germany*

[4]*High Magnetic Field Laboratory, Chinese Academy of Sciences, Hefei, Anhui 230031, People's Republic of China*

[5]*Prokhorov General Physics Institute, Russian Academy of Science, ul. Vavilov 38, 119991 Moscow, Russia*

[6]*Faculty of Physics, M.V. Lomonosov Moscow State University, 119992 Moscow, Russia*

[7]*Moscow Power Engineering Institute, 105835 Moscow, Russia*

[8]*Institut Laue Langevin, 6 rue Jules Horowitz, BP156, F-38042 Grenoble, France*

[9]*Institut de Ciència de Materials de Barcelona, ICMAB-CSIC, Campus Universitari de Bellaterra, E-08193 Bellaterra, Barcelona, Spain*

[10]*Institució Catalana de Recerca i Estudis Avancats (ICREA), E-08010 Barcelona, Spain*

[11]*Departament de Física, Universitat Autònoma de Barcelona, 08193 Bellaterra, Barcelona, Spain*

(Received 31 July 2017; revised manuscript received 6 September 2017; published 25 September 2017)

Slightly Co-doped $MnWO_4$ at the lowest 5% Co concentration, for which the multiferroic cycloidal phase becomes a ground state, has been studied in magnetic fields up to 60 T by bulk magnetic and electric polarization measurements along different crystallographic directions. The field induced magnetic transitions up to 12 T and the ways they proceed were tracked also by single-crystal neutron diffraction, and the relevant field induced magnetic structures were identified and refined. The complete magnetoelectric phase diagrams for magnetic fields along distinct directions in relation to the cycloidal spin structure have been constructed for magnetic field values exceeding those necessary to induce a spin-flip transition into the paramagnetic state. Their common feature is the existence of nonpolar sinusoidal phases identified by the disappearance of the electric polarization in a field regime slightly below the spin-flip transition. At lower magnetic fields either continuous or abrupt field induced reorientations of the cycloidal magnetic structures were observed, respectively, for a field direction along the crystallographic *b* axis or along the easy magnetic axis, and the different character of those transitions has been attributed to specific features in the magnetic anisotropy.

DOI: 10.1103/PhysRevB.96.104435

I. INTRODUCTION

Magnetoelectric multiferroic materials exhibit simultaneously both magnetic and electric orders [1–3]. $MnWO_4$ is considered as an archetypal multiferroic, having a cycloidal magnetic structure with zero net magnetization coexisting with macroscopic electric polarization [4,5]. It belongs to the so-called type II multiferroics, in which both order parameters are inevitably coupled since the magnetic order is what breaks the inversion symmetry and induces ferroelectricity. The main interest in these materials is the possibility of manipulating the polarization by inducing changes in the magnetic structure or vice versa.

Like most of the magnetically frustrated materials, $MnWO_4$ is extremely sensitive to small perturbations induced not only by an external agent such as magnetic field or pressure, but also by chemical substitution. It has been observed [6] that substituting Mn^{2+} by Co^{2+} in $MnWO_4$ enlarges the temperature range where the multiferroic phase of this compound is stable. At 5% of cobalt the low-temperature collinear antiferromagnetic nonpolar phase is suppressed and the multiferroic phase remains stable down to very low temperatures while its average monoclinic crystal structure remains unchanged. The zero-field magnetic structures of this composition have already been described in Refs. [6–8]. Furthermore, a polarization control at spin-driven ferroelectric domain walls was recently demonstrated [9]. On the other hand, in contrast to the pure $MnWO_4$, the evolution of the magnetic structures of $Mn_{0.95}Co_{0.05}WO_4$ under magnetic field is still unclear. The present paper is aimed at describing the magnetic behavior of this material in a large range of magnetic field, revealing how the field induced magnetic structures evolve and also the corresponding evolution of the electric polarization.

It is worth recalling the crystal structure and the zero-field magnetic orders that appear below the Néel temperature in $Mn_{0.95}Co_{0.05}WO_4$. The crystal structure has $P2/c$ monoclinic symmetry (*b* monoclinic axis). Within the unit cell there are two symmetry-related manganese atoms surrounded by deformed oxygen-made octahedra. Those octahedra form zig-zag chains along the crystallographic *c* axis. Below 13.2 K the structure becomes magnetically ordered: between 13.2 and 12.2 K the so-called AF3 phase exists, while below 12.2 K the AF2 multiferroic phase prevails. For the AF3 phase, it has been proposed [10,11] that the most likely magnetic structure is a cycloidal one, where the different chains display a mutually opposite chirality and therefore a zero net electric polarization. Nevertheless, the oscillating spin *y* component is very small (relativistic effect), and the AF3 order is usually considered as an amplitude-modulated collinear sinusoidal structure [10]. As for the AF2 phase, it has a cycloidal spin structure with the moments rotating within the $b\alpha$ plane, α

*irene.urcelay@ehu.eus

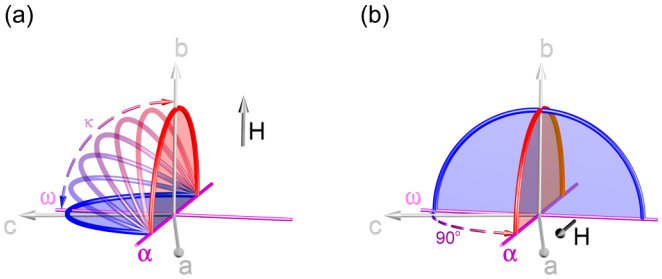

FIG. 1. Sketch of the directions along which the magnetic field was applied: the crystallographic directions a, b, c; the easy α and the hard ω magnetic axes within the ac plane; and the field induced transitions relevant to the AF2 phase (only $H||b$ and $H||\alpha$ are depicted). At 2 K and H=0 this phase has a cycloidal spin structure with the moments rotating within the $b\alpha$ plane (enveloped by the red semicircles), α being located at about 15° from the a towards the c axis, and ω at 90° to α within the ac plane. (a) At 2 K, for $H||b$ a flop of the magnetic moments from the αb to the $\alpha\omega$ plane (i.e., ac plane) occurs *continuously* via a rotation of the cycloid plane around the α (only one of the two directions of rotation is depicted), and κ is the angle between ω and the cycloidal plane. (b) For $H||\alpha$, a flop from the αb to $b\omega$ plane occurs *discontinuously* via a rotation of the cycloid plane around the b axis (only one of the two directions of rotation is depicted). For $H||\omega$ no magnetic field induced transitions take place up to the spin-flip fields (not illustrated).

being the easy-magnetic axis located at about 15° from the a towards the c axis (see Fig. 1). The hard-magnetic axis, ω, is at 90° to α within the ac plane. The latter description corresponds to a simplified picture where the magnetic moments of all Mn atoms are supposed to sit in the same plane. The electric polarization in the AF2 phase is along the b axis. Its origin is well explained by the antisymmetric Dzyaloshinskii-Moriya interaction which induces a local electric polarization $\mathbf{P} \sim \mathbf{r}_{ij} \times (\mathbf{S}_i \times \mathbf{S}_j)$, favored by the noncollinear arrangements of neighboring moments $\mathbf{S}_i$ and $\mathbf{S}_j$ connected by a radial vector $\mathbf{r}_{ij}$ and possessing nonzero spin chirality $\mathbf{S}_i \times \mathbf{S}_j$ [3,12,13]. Field induced changes of the magnetic structure are expected to be accompanied by apparent variations of the electric polarization including its value and orientation.

Here we report a comprehensive study of the various phase transitions in $Mn_{0.95}Co_{0.05}WO_4$ induced by magnetic fields up to 60 T using magnetic, electric polarization, and neutron-diffraction measurements along different crystallographic directions.

II. EXPERIMENTAL DETAILS

Single crystals of $Mn_{0.95}Co_{0.05}WO_4$ were grown by a float-zone method using light heating [14]. The crystal growth was performed in an air atmosphere at a linear speed 8–10 mm/h with a counter-rotation of crystal and feed rod. Finally, the crystal was annealed in air at $T = 1100\,^{\circ}$C for about 6 h. Samples with dimensions suitable for the particular measurements and with different crystallographic orientations were cut from the same crystal.

The magnetic response of the crystal to both, ac and dc magnetic fields was studied using the physical properties measuring system and superconducting quantum interference device from Quantum Design. The magnetic field was applied, within a few degrees of accuracy, along the monoclinic b axis, the magnetic easy, or the hard direction of the crystal (shaped as $5\times2.5\times1$ mm^3 parallelepiped). No measurable frequency dependence was found in the ac susceptibility in the frequency range of 10 Hz to 3 kHz, which was studied at an ac field amplitude of 10 Oe and at different superimposed dc fields up to 9 T. To better monitor the field induced transitions, instead of monitoring the departure from the linear variation of magnetization with the applied dc field, we studied the ac susceptibility at fixed temperatures as a function of the amplitude of the dc field, superimposed in the same direction as the ac field (i.e., the so-called incremental susceptibility).

Electric polarization was studied along the principle crystallographic axes by pyroelectric measurements using a Keithley 6517A electrometer in the static magnetic field measurements. Electrical contacts were attached by Ag paint on the two parallel surfaces of the sample. A poling field, E_p, up to ±1.4 kV/cm was first applied in the paraelectric state at temperature 15–20 K prior to cooling the sample through the Néel temperature down to 1.9 K in order to obtain a single polar domain state. This electric field was maintained during the magnetic field or temperature-dependent polarization experiments. The temperature dependence of polarization upon heating or cooling was measured in swiping the temperature mode with a rate of about 1 K/min, resulting in a small hysteresis of less than 1 K.

The high magnetic field experiments were performed at the Dresden High Magnetic Field Laboratory. Pulsed magnetic fields up to 60 T with pulse duration of 35 and 150 ms were used. The magnetization was measured by integrating the voltage induced in a coil system surrounding the sample. The system was precisely compensated before the pulse to cancel the dB/dt contribution. Electric polarization, $\mathbf{P}$, was measured by a pyroelectric technique [15]. The pyrocurrent was captured through the voltage variation in a shunt resistor connected in series with the measurement circuit by a digital oscilloscope Yokogawa DL750 with a high sampling rate of 1 MS s^{-1} and a resolution of 16 bit. Then, $\mathbf{P}$ was calculated by integrating the pyrocurrent numerically. Magnetic field dependencies were usually recorded with electric field (equal to the poling field of about 1.4 kV/cm) switched on in attempt to secure a single domain structure after the field induced transitions. The sample used in the above high-field experiments was shaped as a parallelepiped (pseudocub) with ~1.8-mm-long edges along the easy and the hard magnetic axis, and the b axes.

The neutron-diffraction experiments were carried out on the CEA-CRG D23 single-crystal diffractometer at the Institut Laue Langevin (Grenoble, France). The same crystal, which was used for the bulk magnetic measurements, was mounted inside a vertical cryomagnet and investigated with an incident wavelength λ=1.277 Å. Two different sample orientations have been employed: first the crystallographic b axis was set vertical with respect to the laboratory frame of reference, and afterwards the easy axis was set vertical. The neutron absorption in the sample ($\mu = 0.041\text{mm}^{-1}$) has been corrected using the Cambridge Crystallography Subroutine Library [16] and the structure refinements were done using the FULLPROF SUITE package [17]. Data treatments were done by least-square

refinements of the integrated intensities and they included an extinction correction following the model of Becker-Coppens [18]. For determining the magnetic structures, the crystallographic parameters and the scale factors were fixed to the values obtained in the nuclear refinements. The spin configurations have been described as follows: For a given magnetic propagation vector $\mathbf{k}$ (and the associated $-\mathbf{k}$)

$$\mathbf{m}_{lj} = m_{1j}\hat{u}_j \cos[2\pi(\mathbf{k}\cdot\mathbf{R}_l + \Phi_j)] + m_{2j}\hat{v}_j \sin[2\pi(\mathbf{k}\cdot\mathbf{R}_l + \Phi_j)] \quad (1)$$

where $\mathbf{m}_{lj}$ is the magnetic moment of the atom j in the unit cell l, $\mathbf{R}_l$ is the vector joining the arbitrary origin to the origin of unit cell l, and Φ_j is a magnetic phase [19].

III. RESULTS AND DISCUSSION

A. Field induced transitions at moderate fields ($H < 15$ T)

1. Probing field induced transitions by incremental magnetic susceptibility

To detect field induced transitions, ac susceptibility was measured along different directions at fixed temperatures when varying the amplitude of the dc field (limited to 9 T) which was superimposed in the same direction as the ac field. Figure 1 shows a sketch of the directions in which the magnetic field was applied: the three principle crystallographic directions, the easy α and the hard ω magnetic axes within the ac plane. It also illustrates the transitions induced in moderate magnetic fields which will be discussed further in the paper. The evolution of the incremental susceptibility at 1.8 K shown in Fig. 2 reveals a field induced transition for the $H||b$ direction and suggests a beginning of such transition along the α easy direction, while no indication of any transition is seen along the hard axis up to the highest applied field.

The transition with $H||b$ starts at fields of about 3.5 T, as indicated by the increase of the real component of the ac susceptibility in Fig. 2, and ends at about 7 T. The susceptibility evolution suggests that this transition is completed in two

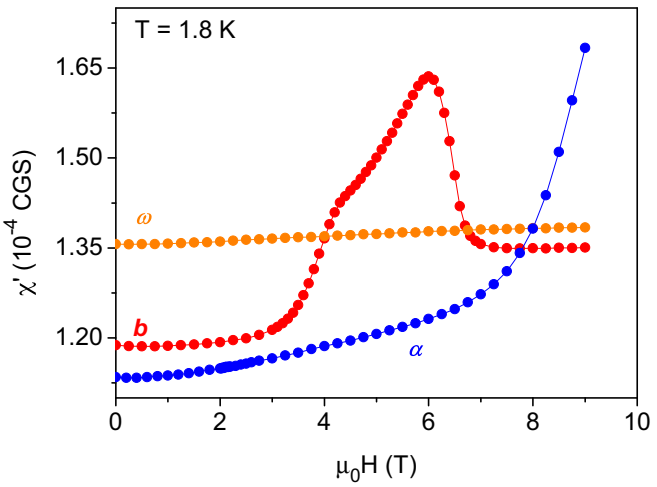

FIG. 2. Real component of the ac susceptibility vs superimposed dc field along the α easy and the ω hard magnetic directions, and along the b axis, obtained at 1.8 K.

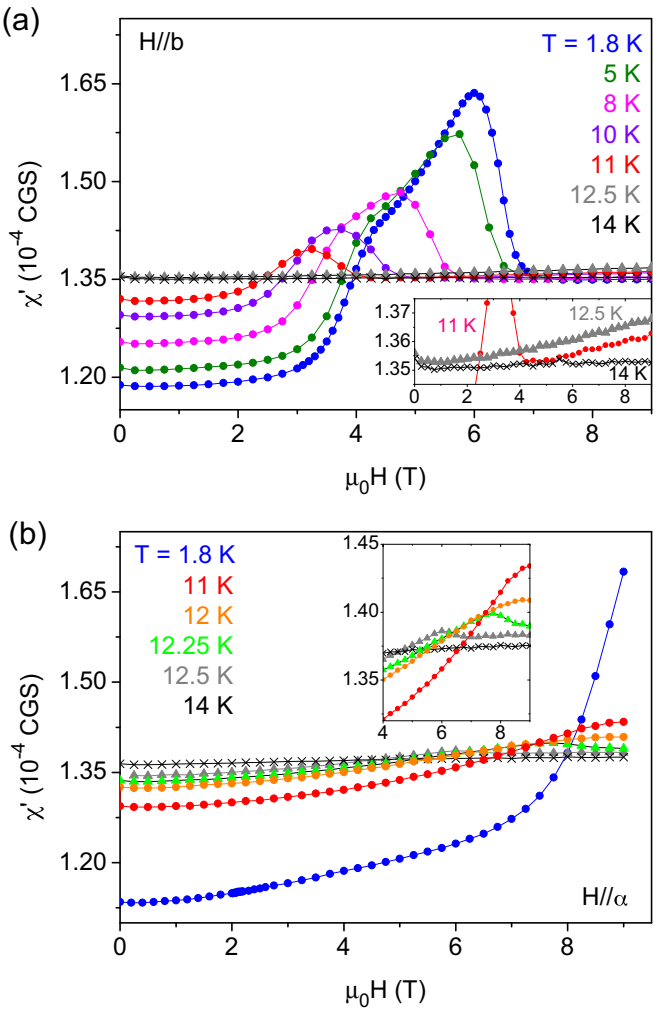

FIG. 3. Real component of the ac susceptibility along b crystallographic and α easy magnetic axes vs superimposed dc field, at different temperatures—panel (a) and (b), respectively. The insets are zooms. Temperatures at which (at zero magnetic field) the AF2 phase, the AF3 phase, or the paramagnetic phases exist are represented by full circles, triangles, and crosses, respectively.

stages, evidenced by the susceptibility increase from the practically constant low-field values, followed by an almost linear increase and then a decrease to a roughly constant value at high field. The higher the temperature is, the lower the field needed to induce the transition is and the narrower the transition itself is [see Fig. 3(a)]. The two consecutive stages seem to merge into a single one at temperatures above 8 K. In the AF3 phase, between about 12.1 and 13.2 K, the peak in the susceptibility completely disappears and the slope of the curves coincides with the slope of the high-field phase of the AF2 structure [see the inset of Fig. 3(a)]. In the paramagnetic region (14 K), as expected, the susceptibility is practically constant.

A field induced transition takes place also for the $H||\alpha$ easy direction. As seen from Fig. 2, at 1.8 K, the susceptibility initially increases almost linearly up to about 7 T followed by much faster increase at higher fields indicating the beginning of the transition, which, however, remains uncompleted up to the highest field available of 9 T. The susceptibility maxima [see the inset of Fig. 3(b)] observed on the 12, 12.25, and

12.5 K curves (AF3 phase region) should be related to the crossing from AF3 either to a spin-flopped AF3" phase or to the paramagnetic region. This will be further argued when presenting the high-field data.

2. *Continuous rotation of the magnetic structure and the electric polarization with H||b*

The first step in the neutron study of the evolution of the magnetic structure under magnetic field applied along the *b* axis was to follow the behavior of two magnetic reflections as the field increased at a fixed temperature of 2 K. The integrated intensities of those reflections, namely, $(0\,0\,0)^{+\mathbf{k}}$ and $(0\,0\,1)^{-\mathbf{k}}$, depicted in Fig. 4(a), exhibit changes in the field range 2.5–7 T, which agree with the field induced transition observed by means of ac susceptibility measurements with $H||b$. The $(0\,0\,0)^{+\mathbf{k}}$ reflection shows an evolution characterized by a maximum and a minimum intensity value that occur at the fields where the $(0\,0\,1)^{-\mathbf{k}}$ starts increasing and has a maximum, respectively.

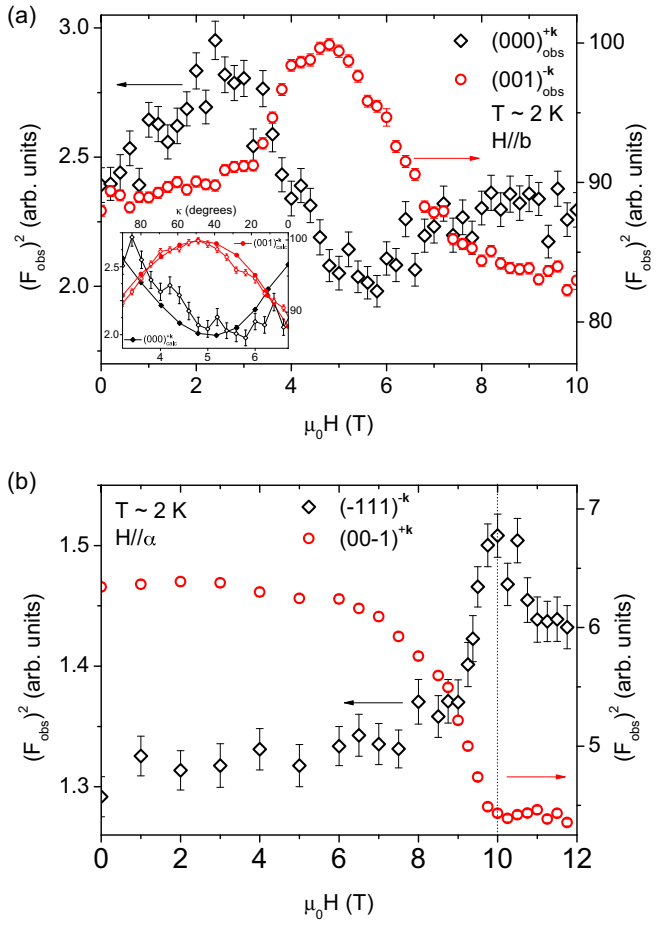

FIG. 4. (a) The experimental integrated intensities of $(0\,0\,0)^{+\mathbf{k}}$ and $(0\,0\,1)^{-\mathbf{k}}$ reflections as a function of the magnetic field applied along the *b* axis at 2 K. Inset: Zoom of the field range 3–7 T, including also the calculated intensities (full symbols) for those reflections as a function of the angle κ between the cycloidal plane and the hard direction ω in the *ac* plane. (b) The experimental integrated intensities of $(0\,0\,-1)^{+\mathbf{k}}$ and $(-1\,1\,1)^{-\mathbf{k}}$ reflections as a function of the field applied along the easy direction α at 2 K.

TABLE I. Refined parameters of $Mn_{0.95}Co_{0.05}WO_4$ magnetic structures at zero field, 5 T, and 10 T (2 K, $H||b$). For simplicity the following notation has been used: $\mathbf{k}_0 = [-0.216(1), \frac{1}{2}, 0.461(1)]$ and $\mathbf{k}_b = [-0.216(2), \frac{1}{2}, 0.460(2)]$. The unitary vectors $\hat{u}$ and $\hat{v}$ are described by spherical angles: ϕ is the angle that the projections of the unitary vectors in the xy plane make with x ($||a$) and θ is the angle the unitary vectors make with z ($||c^*$). $\Delta\Phi$ corresponds to the magnetic phase difference of Mn_1 and Mn_2. κ is the angle between the plane where moments lay and the hard direction ω in the *ac* plane; it is not refined but derived from ϕ_v and θ_v. The data set collected at 5 T was refined in two different ways: in the first one the easy axis was fixed ($\hat{u}$) and only the orientation of $\hat{v}$ was refined, whereas in the second refinement the orientation of both vectors was refined. m_{1j} and m_{2j} correspond to the modulus of the two oscillating orthogonal components of magnetic moments shifted 90° in phase. $R_{F^2}/\%$, $R_{F^2w}/\%$, $R_F/\%$, and χ^2 are the reliability factors.

Temperature:		2 K	2 K	2 K	2 K
Magnetic Field:		0 T	5 T	5 T	10 T
k		$\mathbf{k}_0$	$\mathbf{k}_b$	$\mathbf{k}_b$	$\mathbf{k}_b$
Mn_1	$m_{1j}\mu_B$	3.83(7)	3.88(3)	3.86(4)	3.91(6)
	ϕ_u	0°	0°	0°	0°
	θ_u	77(2)°	77°	64(4)°	86(2)°
	$m_{2j}\mu_B$	−3.89(6)	−3.43(4)	−3.35(4)	−3.30(4)
	ϕ_v	90°	106(3)°	124(4)°	180°
	θ_v	90°	32(3)°	46(4)°	−4°
Mn_2			$\hat{u}_{Mn_2} = -\hat{u}_{Mn_1}$		
			$\hat{v}_{Mn_2} = -\hat{v}_{Mn_1}$		
$\Delta\Phi$		$k_z/2$	$k_z/2$	$k_z/2$	$k_z/2$
κ		90°	32(4)°	37(4)°	0°
$R_{F^2}/\%$		11.8	12.3	11.5	14.5
$R_{F^2w}/\%$		10.0	9.58	8.71	13.1
$R_F/\%$		16.1	17.2	16.8	19.0
χ^2		10.2	8.40	7.00	4.01
Note			Fixed α	Free α	

Centering of roughly 20 magnetic reflections at 5 and 10 T led us to conclude that the propagation vector ($\mathbf{k}_b = [-0.216(2), \frac{1}{2}, 0.460(2)]$) practically remains unchanged in comparison to the one found at zero field ($\mathbf{k}_0 = [-0.216(1), \frac{1}{2}, 0.461(1)]$). The magnetic structures were refined from the integrated intensities of about 130 reflections [20], at 5 and 10 T, i.e., at a magnetic field value at which the transition takes place and at another in which the transition is completed, respectively, as indicated by the susceptibility measurements (see Fig. 2). The parameters that describe the proposed spin arrangements are gathered in Table I. The data treatment concluded that the high-field structure ($\mu_0 H = 10$ T) is a cycloidal structure in the *ac* plane, perpendicular to the external field, as expected for an antiferromagnet at fields above the spin-flop transition. Hereafter AF2' will be used for this phase. The treatment of the data recorded at 5 T, i.e., in an intermediate field, revealed that the magnetic structure is such that the rotation plane of the moments is in between the initial and final orientations, and hence suggests that the transition occurs in a continuous manner. Taking into account the refinement at 5 T, the plane in which the moments rotate tilts around the easy axis (α): one can observe in

Table I that by fixing the easy axis and leaving the rest of the parameters free in the refinement the plane rotates around α towards the ac plane making an angle of $\kappa = 32(4)^\circ$ with the ac plane. However, if we give more freedom to the structure, and refine the parameters associated to the easy axis too, it slightly tilts towards c. In this last model the angle κ is bigger, $46(4)^\circ$.

The evolution of the magnetic reflections in Fig. 4(a) has been simulated based on the proposed model for the transition, i.e., by considering that the plane rotates around α. The simulation has been done just considering the rotation of the $\hat{v}$ vector, maintaining constant its modulus and the orientation and modulus of $\hat{u}$. The inset of Fig. 4(a) presents the experimental integrated intensities of the $(0\ 0\ 0)^{+\mathbf{k}}$ and $(0\ 0\ 1)^{-\mathbf{k}}$ reflections (represented by empty symbols) as a function of the external field and their calculated intensities (full symbols) as a function of κ. The resulting evolution of the intensities of the observed reflections is satisfactorily reproduced just by modeling the transition with one parameter, κ. Therefore, in a first approximation, the behavior of the magnetic reflections holds that the transition between the magnetic structures can be described as a continuous rotation of the plane of the moments around the magnetic easy axis. Note that the higher-order effects revealed by the refinements, such as the small reorientation of the easy axis or the variation of the amplitudes, were not taken into account in the simulation and could be at the origin of the offset between κ and the field in the refinements and the simulation.

Figures 5(a) and 5(b) show the field dependence of the a, b, and c components of the electric polarization at different temperatures, in $H||b$ configuration. A smooth decrease of P_b is observed starting at ∼3.5 T and finishing at ∼7.5 T (data taken at 4.2 K), in good agreement with the other techniques we used. As observed in the susceptibility measurements, the width of the transition decreases with increasing temperature and this is also reflected in the polarization measurements (note that P_b at 10 K disappears within the 3 T field range). Polarization P_b exhibits a small hysteresis with the field. On cycling the magnetic field it reaches the same zero-field value, thus suggesting a polar single domain state or at least establishing the same balance between magnetic domains with opposite chirality when coming from high temperature in zero magnetic field and on cycling the field at a fixed temperature (we recall the presence of an electric field in both experiments). Both a and c components of the polarization rise at about 3 T and reach their maximum at about 6.5 T (at 4.2 K). These results agree with the continuous flop of the rotation plane of the moments upon the AF2-to-AF2' transition. In the initial and final stages of the phase transition, the electric polarization is either along b or in the ac plane, whereas in the intermediate stages it has nonzero components along all the three principle crystallographic directions. One may argue that this can be due to a phase separation and therefore a result of the contribution of two polar magnetic structures each of which producing polarization either along b or in the ac plane. However, the magnetic-diffraction data refinement concluded that there is a unique ferroelectric phase in which the rotation plane of the moments is in between the $b\alpha$ and the ac plane, keeping always the direction of the easy axis α, $\mathrm{AF2}^{\mathrm{ang}}(P_a, P_b, P_c)$, and hence the hypothesis of the phase separation can be ruled out.

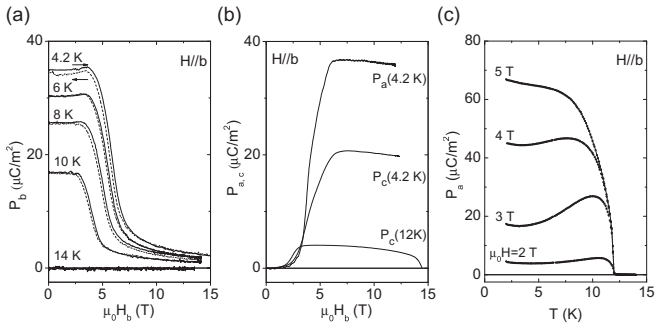

FIG. 5. Field dependence of the components of the electric polarization along the principle crystallographic directions for $H||b$. (a) P_b component at several temperatures and (b) P_a and P_c components at 4.2 K. (c) Temperature dependence of P_a at different fields.

The electric polarization along the a axis, P_a, was measured also as a function of the temperature at fixed fields parallel to b. The data plotted in Fig. 5(c) suggest that at moderate magnetic fields the temperature of the onset of electric polarization remains unchanged. The behavior of the polarization is rather peculiar: at low fields, it has a maximum value close to T_{FE} and decreases at low temperatures. In the work by Liang *et al.* [8] this interesting response to the temperature of P_a, that occurs at fields between 2 and 5 T, is associated to the rotation of the spin plane around the easy axis. The authors suggest that in this field range and right below T_{FE}, the spin plane is parallel to ac, and then, with decreasing temperature the plane rotates. The temperature range where the reorientation of the plane takes place depends on the field; for example, at 2 T, P_a tends to zero within 2 K. In contrast, at 4 T none of the components of the polarization is zero and therefore, at that field, the rotation of the spin plane is not completed.

3. *Transitions induced with the $H||\alpha$ easy axis*

Susceptibility measurements with $H||\alpha$ suggest the beginning of a field induced transition, presumably a spin flop of the cycloidal plane (see Fig. 1), that is probably completed slightly above the maximum available field of 9 T for this measurement (this will be further confirmed by the pulsed high-field data in Sec. III B 2). This reorientation is due to a competition of the Zeeman with the crystallographic magnetic anisotropy term in the free energy. At zero field the latter stabilizes the cycloidal structure located in the easy αb plane. With increasing the field along the easy α axis this direction of the spins becomes unstable, which results in a reorientation of the cycloidal plane presumably to the $b\omega$ plane (perpendicular to the field).

In the neutron-diffraction study, first two magnetic reflections were monitored at 2 K as the field increased from 0 to 12 T. The evolution of the integrated intensities of those two reflections displays a clear and sharp transition at 10 T [see Fig. 4(b)]. The intensity of the $(0\ 0\ -1)^{+\mathbf{k}}$ reflection gradually decreases until the transition occurs, then it remains constant up to 12 T. In contrast, the intensity of the $(-1\ 1\ 1)^{-\mathbf{k}}$ reflection increases and has a maximum value at 10 T, then it decreases and above 11 T it becomes constant too. Magnetic Bragg peak intensities were collected at 8 (before the transition), 10, and

11.75 T (above the transition). Unfortunately, the collected data at both high field and intermediate fields did not allow us to determine unambiguously the corresponding magnetic phases. Due to the geometrical restrictions imposed by the magnet, the number of collected reflections was not enough to give a definitive answer.

B. Field induced transitions at high fields (up to 60 T)

With anticipation to reach the field-forced ferromagnetic alignment (i.e., paramagnetic state) and consequently accessing all possible field induced transitions, the field range in this paper was extended by using pulsed magnetic fields up to 60 T at the European High Magnetic Field Laboratory facilities in Dresden to measure magnetic susceptibility and the pyrocurrent.

1. Transitions induced with H||b

Figure 6(a) shows the evolution of the magnetic susceptibility in fields along the b axis, while the magnetization obtained by integrating the corresponding susceptibility curves is plotted in Fig. 6(b). The clear magnetization change on the 1.5 K data at about 58 T [Fig. 6(b)] is indicative for reaching the spin-flip field. The forced ferromagnetic alignment of the moments above this field value is reflected in magnetization saturation and consequently the susceptibility tends to zero [see Fig. 6(a)]. The estimated magnetic moment per formula unit is $\approx$4.4 μ_B, which is somewhat smaller than 4.9 μ_B, expected from Mn^{2+} ($S = 5/2$) and Co^{2+} ($S = 3/2$) spin only moments. However, this difference should be taken with some precautions since it might result, at least partly, from inaccuracy in the calibration of the high-field magnetization when using the low dc field data. As expected, with increasing temperature the spin-flip field decreases and is smeared out due to the thermal fluctuations opposing the collinear alignment of the magnetic moments along the direction of the applied field. This intrinsic feature affects the accuracy in determining the spin-flip fields at the higher temperatures.

The above transition is expected to occur via an intermediate (magnetic sinusoidal, which is paraelectric) phase, i.e., following the sequence: cycloidal AF2'→ AF3 (intermediate sinusoidal magnetic structure) → forced ferromagnetic state.

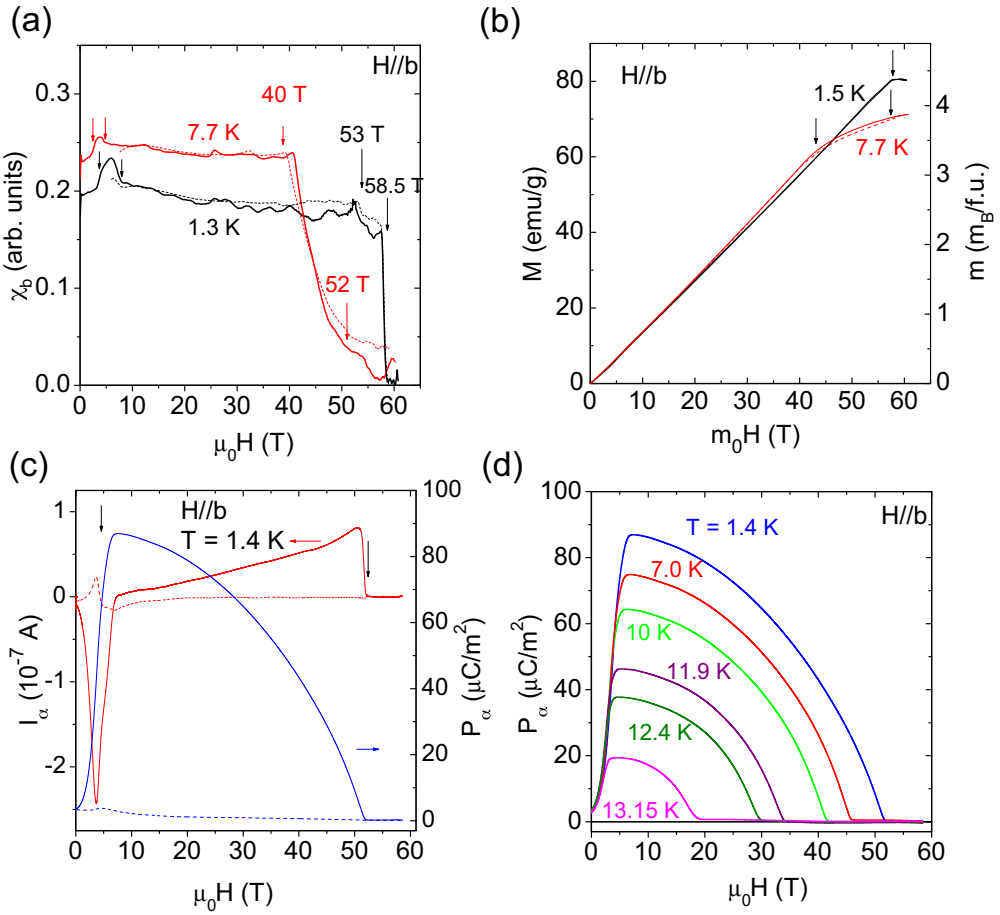

FIG. 6. $H||b$ case: (a) Magnetic susceptibility, χ_b, in pulsed magnetic field along the b axis. Low-field anomalies (~4-6 T) correspond to continuous rotation of the spin cycloid from αb to ac plane, while the high-field ones can be identified as a transition to the forced ferromagnetic (paramagnetic) state occurring presumably via an intermediate (sinusoidal paraelectric) phase. (b) Magnetization curves $M_b(H)$ obtained by integration $\chi_b(H)$ and scaled using the low-field (up to 9 T) magnetization data. (c) The evolution of the pyrocurrent (left scale) and the electric polarization (right scale) along the α axis on the pulsed magnetic field applied along the b axis. (d) Electric polarization $P_\alpha(H)$ for selected temperatures, recorded at magnetic field decreasing. Solid and dashed lines are for decreasing and increasing magnetic field branches, respectively. The vertical arrows tentatively indicate the expected field induced transitions.

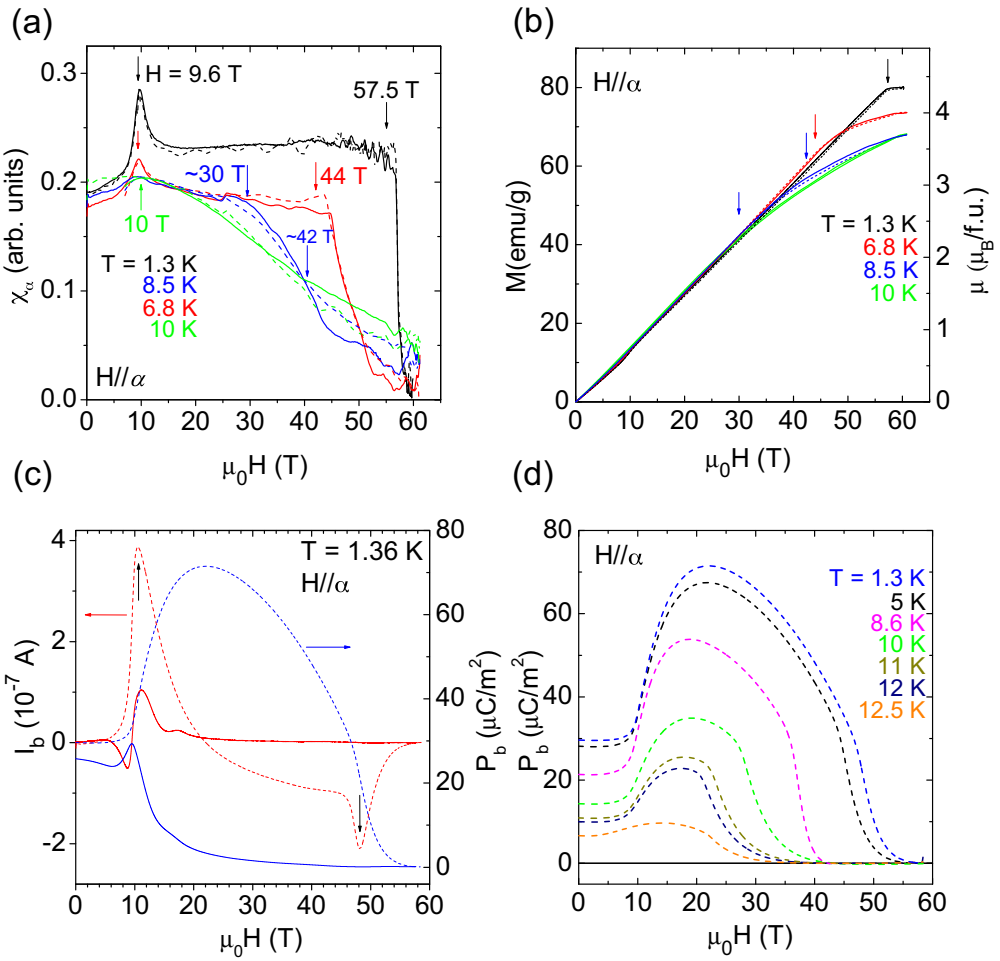

FIG. 7. $H||\alpha$ case. (a) Evolution of the magnetic susceptibility in fields along the easy magnetic axis α, $\chi_\alpha(H)$. Low-field anomaly (∼9.6 T) corresponds to the flop of the spin cycloid to the plane perpendicular to the easy axis. The high-field features can be identified as a transition to the forced ferromagnetic (paramagnetic) state, which is expected to occur via an intermediate (sinusoidal, paraelectric) phase. (b) Magnetization curves $M_\alpha(H)$ obtained by integration $\chi_\alpha(H)$ and scaled using the static (up to 9 T) magnetization data. (c) The evolution of the pyrocurrent (left scale) and the electric polarization (right scale) along the a axis on the pulsed magnetic field applied along the b axis. Vertical arrows indicate threshold fields of the phase transitions. (d) Electric polarization $P_b(H)$ for selected temperatures, recorded as the magnetic field decreased. Solid and dashed lines are for decreasing and increasing magnetic field branches, respectively. Arrows illustrate possible identification of these high-field transitions.

However, it is not easy to identify all corresponding anomalies from the $\chi_b(H||b)$. Arrows in Fig. 6(a) indicate a tentative identification of these high-field transitions being in reasonable agreement with the electric polarization measurements (as will be discussed below).

A low-field (∼4−6 T) anomaly on the susceptibility is also observed in agreement with the static field data presented in Sec. III A. The two stages of the anomaly, clearly seen on the static-field susceptibility and attributed to the beginning and the end of the continuous rotation of the spin cycloid from the αb to the ac plane at the AF2-to-AF2' transition (see Sec. III A 2), could be clearly appreciated on the pulsed field data.

The above low-field transition is also manifested on the field dependence of the pyrocurrent $I_\alpha(H||b)$, plotted in Fig. 6(c), though its details are not so well expressed as on the P_a data presented in Fig. 5, measured in static or in pulsed fields with significantly smaller dH/dt (please also keep in mind the small, some 15°, difference between the α and the a geometries). Figure 6(c) includes also the corresponding polarization evolution, $P_\alpha(H||b)$, which appears at the low-field AF2-to-AF2' transition and disappears at about 52 T. This latter value is lower than the spin-flip field of 58 T determined from the magnetic data and thus supports the hypothesis for the existence of an intermediate magnetic phase, most likely a sinusoidal collinear magnetic configuration, which separates the cycloidal and the paramagnetic phases. Note that this latter intermediate state does not support electric polarization. It is worth noting the huge difference between the ascending and the descending field branches of the polarization. This implies that the true maximum value of the P_α polarization is achieved only when the AF2' phase is entered from the nonpolar phase (the forced ferromagnetic or the proposed intermediate sinusoidal one) on reducing the magnetic field and in the presence of an electric field ensuring a single polar state. Note that this maximum P_α polarization value

is much bigger than the one established after the AF2-to-AF2' transition in the presence of the same electric field.

The field evolution of the P_α polarization at several temperatures is gathered in Fig. 6(d) for decreasing field.

2. *Transitions induced with the H||α easy axis*

Figure 7(a) shows the evolution of the magnetic susceptibility in fields along the easy magnetic axis α, while the magnetization obtained by integrating the corresponding susceptibility curves is plotted in Fig. 7(b). The high-field features can be identified as a transition to the forced ferromagnetic (paramagnetic) state, which is expected to occur via an intermediate (sinusoidal, paraelectric) phase. It is plausible to identify this phase with a flopped AF3 phase, which we will denote as AF3". The low-field anomaly (∼9.6 T) corresponds to the flop of the αb spin cycloid to the plane perpendicular to the easy axis AF2-to-AF2", as discussed in Sec. III A 3.

Both, the low-field transition AF2 → AF2" and the high-field AF2"→ sinusoidal phase one are manifested in the field dependence of the b component of the pyrocurrent in the $H||\alpha$ configuration $I_b(H||\alpha)$ at 2 K, plotted in Fig. 7(c) together with the correspondent field evolution of $P_b(H||\alpha)$. Upon initial increasing of the magnetic field, $P_b(H||\alpha)$ sharply rises at the AF2 → AF2" transition and goes through a broad maximum before vanishing in the high-field sinusoidal state. One notices a striking difference in how the polarization evolves at the ascending/descending field branches for this spontaneous P_b component recorded in $H||\alpha$ and the magnetic field induced P_α component in $H||b$: namely, unlike the $P_\alpha(H||b)$ case (see Sec. III B 1), the $P_b(H||\alpha)$ ascending branch value is much bigger than the value for the descending branch for fields exceeding the spin flip. The different behavior in the last case $P_b(H||\alpha)$ could be due to the existence of the spontaneous polarization $P_b(H=0)$ the maximum value of which is established by a poling procedure and results in a single chirality state remaining in the spin-flopped phase AF2". The field evolution of P_b polarization at several temperatures is presented in Fig. 7(d).

3. *Transitions induced with the H||ω hard axis*

As expected in analogy with the more simple case of a collinear antiferromagnet, at $H||\omega$, i.e., parallel to the hard

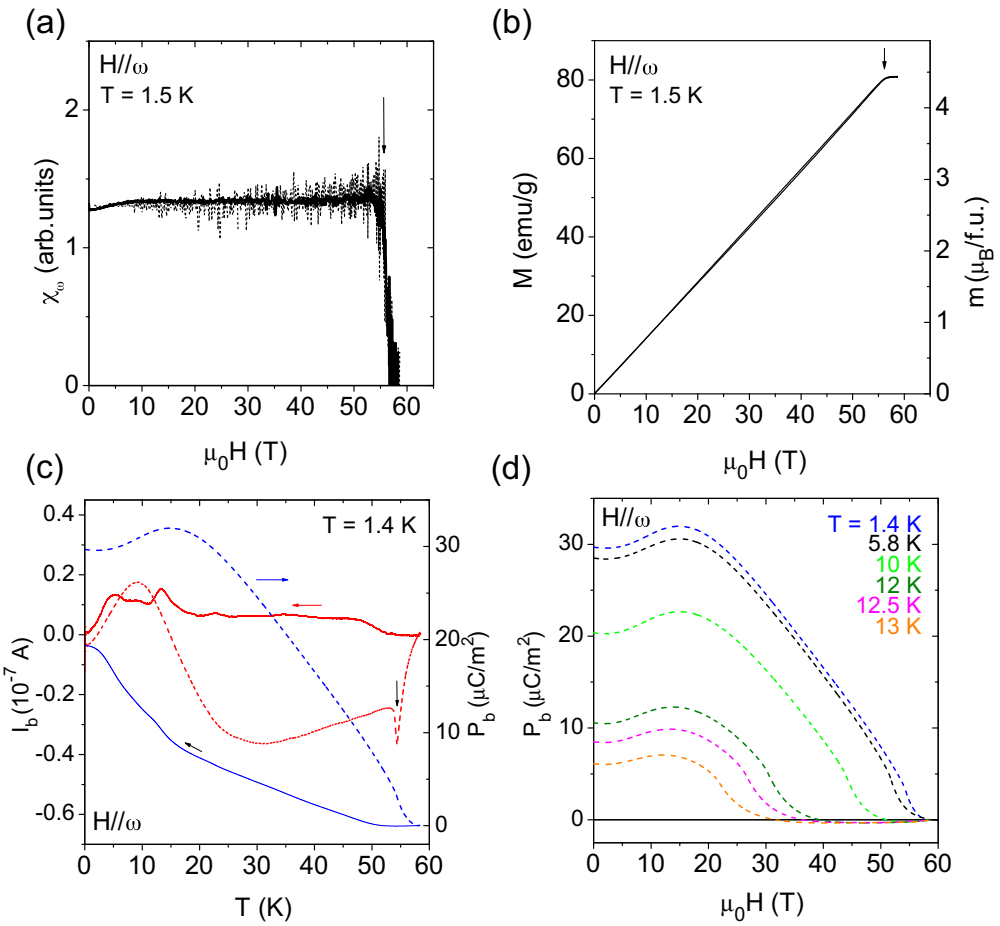

FIG. 8. $H||\omega$ case: (a) Evolution of the magnetic susceptibility in fields along the hard magnetic axis ω within the ac plane, $\chi_\omega(H)$. The arrows illustrate the spin-flip transition. (b) Magnetization curve $M_\omega(H)$ obtained by integration of $\chi_\omega(H)$ and scaled using the static (up to 9 T) magnetization data. (c) The evolution of the pyrocurrent (left scale) and the electric polarization (right scale) along the ab axis on the pulsed magnetic field applied along the hard magnetic axis ω within the ac plane. Vertical arrows indicate threshold field to the paraelectric state. (d) Electric polarization $P_b(H)$ for selected temperatures, recorded at magnetic field decreasing. Solid and dashed lines are for decreasing and increasing magnetic field branches, respectively.

magnetic axis, no magnetic field induced transitions were observed up to the spin-flip field of about 58 T, a value similar to that found for the other two directions [see Fig. 8(a)]. The spontaneous b component of the electric polarization $P_b(H||\omega)$ shows [Fig. 8(b)] the same behavior on increasing/decreasing magnetic field as in the $H||\alpha$ case, i.e., as the field increases, the polarization along b is much bigger than its value when the field descends from fields exceeding the spin flip. The field evolution of the P_b polarization at several temperatures is presented in Figs. 8(c) and 8(d).

IV. PHASE DIAGRAMS AND SUMMARY

The critical fields probed by the different experiments described above and denoted by arrows in Figs. 6–8 have been used to construct the magnetoelectric phase diagrams for magnetic fields along the crystallographic b direction, and the two distinct magnetic directions α and ω [see Figs. 9(a)–9(c)]. A common feature of all phase diagrams is the existence of the nonpolar sinusoidal phases (AF3, AF3") which were clearly identified by the disappearance of the electric polarization at threshold fields below the spin-flip ones. These phases should have a sinusoidal component (orthogonal to the field direction) along the easy (α) axis (AF3) or intermediate (b) axis (AF3"), respectively for $H||b$, ω and $H||\alpha$. Evidences of such nonpolar sinusoidal phases were also observed experimentally in pure $MnWO_4$ [21] and confirmed by a simulation of the $H-T$ phase diagrams [22–24]. The appearance of the field induced nonpolar sinusoidal phases (AF3 or AF3") from the polar cycloidal ones (AF2, AF2', AF2") can be qualitatively explained by a progressive canting of the antiferromagnetic structure, caused by increasing the Zeeman energy with respect to the exchange term. This results in a recovery of the phase transformation sequence (cycloidal $\rightarrow$ sinusoidal $\rightarrow$ paramagnetic), similar to the temperature induced spontaneous one at $H = 0$ (i.e., AF2 $\rightarrow$ AF3 $\rightarrow$ paramagnetic). The analogy with spontaneous transitions is supported by the fact that the antiferromagnetic order parameters are reduced either by increasing temperature or by increasing magnetic field.

At lower magnetic fields a competition of the Zeeman energy with the magnetic anisotropy becomes of primary importance and governs the transformation of the magnetic structures for $H||b$ and α axes. Magnetic field applied in the spin cycloidal plane, i.e., along the b direction or the easy α axis, results in an instability and flop of the spontaneous cycloidal magnetic structure oriented in the αb plane. However, the character of the instability and the transformation depends on the field orientation. For $H||\alpha$ the cycloidal plane rotates abruptly around the b axis to a state perpendicular to the field direction (similarly to a usual spin-flop transition), while for $H||b$ the flop to the $\alpha\omega$ plane (i.e., ac plane) occurs continuously via a rotation of the cycloid plane around the α axis and the corresponding magnetic cycloidal structure could be identified as an angular one, $AF2^{ang}$, where the angle κ, between the plane where the moments lay and the ac plane, varies between 90 (AF2) and 0° (AF2') (Fig. 1). The continuous character of the spin cycloid induced reorientation in $H||b$, which was also observed in Ref. [8], suggests the presence of fourth-order magnetic anisotropy terms needed to stabilize the angular $AF2^{ang}$ phase (in addition to the

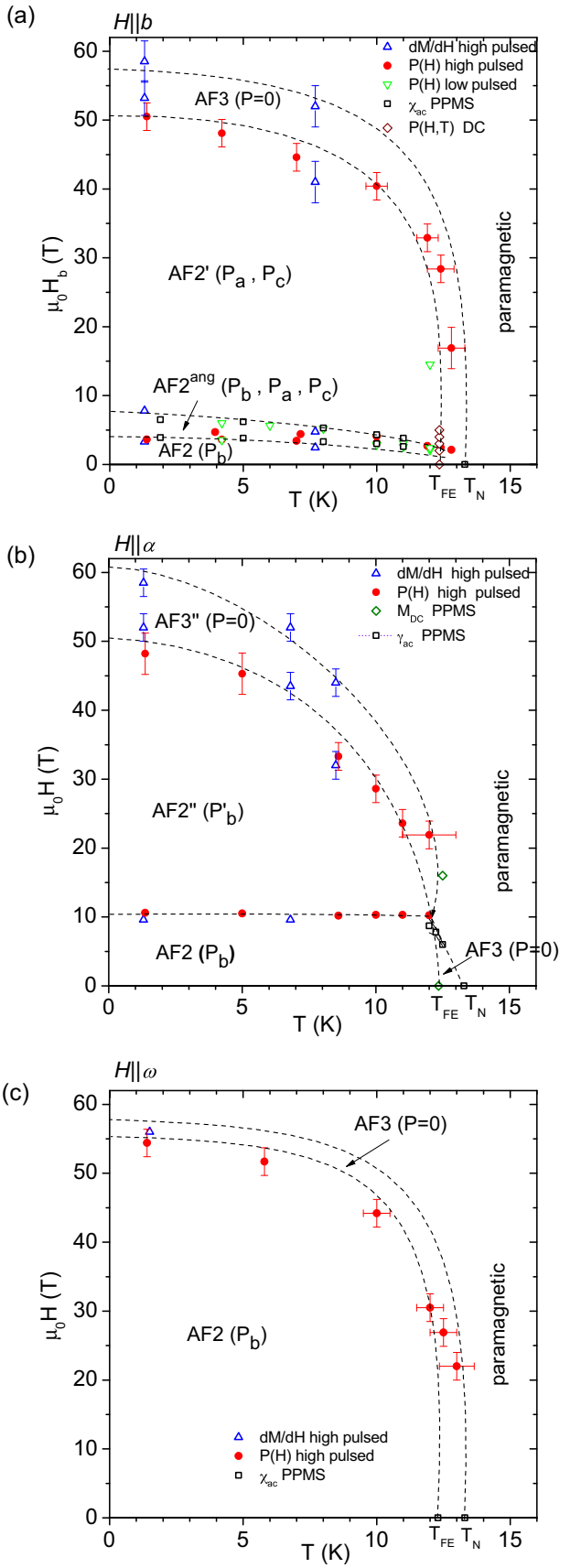

FIG. 9. Magnetic field temperature phase diagrams for magnetic field along b axis (a), easy axis in the ac plane (b), and hard axis in the ac plane (c).

second-order terms). A possible origin of higher-order terms in the Co substituted $MnWO_4$ compounds could be related to the presence of intrinsic competition between the exchange and the anisotropy of the Mn^{2+} and Co^{2+} ions. As a matter of fact, recent x-ray magnetic scattering experiments [25] indeed reveal some local noncollinearity of Mn and Co spins in the commensurate antiferromagnetic AF4 phase of $Mn_{0.85}Co_{0.15}WO_4$. The description of the system in terms of averaged magnetic order parameters (angles) requires averaging the free energy, which is a function of locally fluctuated order parameters. This results in a renormalization of the different terms in the free energy, including the anisotropy energy one and even in appearance of additional fourth-order terms in it (see, for example, Refs. [26,27]). How it could be applied to our system requires a detailed microscopic analysis of the Mn and Co contributions and is beyond the frame of this paper. However, we note that the key effect of the light Co substitution is a reduction of the anisotropy in the αb plane as compared to the pure $MnWO_4$. This results in stabilizing of the cycloidal structure AF2 down to the lowest temperatures and suppression of the commensurate collinear AF1 phase. The noticeable decrease of the anisotropy in the $b\omega$ plane results in lowering of the spin-flop field along the b axis as compared to the $MnWO_4$. Elucidating how each of the two distinct magnetic atoms, sharing the same crystallographic site in the structure and displaying competing anisotropies, behaves at a local scale would require further experimental efforts.

ACKNOWLEDGMENTS

We acknowledge support from the Institute Laue Langevin (Grenoble) for the neutron-diffraction experiments and support from HLD at HZDR, a member of the European Magnetic Field Laboratory, for the high magnetic field experiments. Financial support from the Spanish Ministry of Economy and Competitiveness, through Projects No. MAT2015-68760-C2-2-P and MAT2015-66441-P (cofunded by ERDF of European Union) and No. MAT2017-85232-R, and the Severo Ochoa Programme for Centres of Excellence in R&G (Project No. SEV-2015-0496) is also acknowledged. This paper was partially supported by the Russian Scientific Foundation (Project No. 16-12-10531). Z.W. acknowledges support from the Chinese Academy of Sciences via the One-Hundred Talent program.

[1] T. Kimura, T. Goto, H. Shintani, K. Ishizaka, T. Arima, and Y. Tokura, Nature (London) **426**, 55 (2003).
[2] S. W. Cheong and M. Mostovoy, Nat. Mater. **6**, 13 (2007).
[3] H. Katsura, N. Nagaosa, and A. V. Balatsky, Phys. Rev. Lett. **95**, 057205 (2005).
[4] K. Taniguchi, N. Abe, T. Takenobu, Y. Iwasa, and T. Arima, Phys. Rev. Lett. **97**, 097203 (2006).
[5] A. H. Arkenbout, T. T. M. Palstra, T. Siegrist, and T. Kimura, Phys. Rev. B **74**, 184431 (2006).
[6] Y.-S. Song, J.-H. Chung, J. M. S. Park, and Y.-N. Choi, Phys. Rev. B **79**, 224415 (2009).
[7] F. Ye, S. X. Chi, J. A. Fernandez-Baca, H. B. Cao, K. C. Liang, Y. Q. Wang, B. Lorenz, and C. W. Chu, Phys. Rev. B **86**, 094429 (2012).
[8] K.-C. Liang, R. P. Chaudhury, Y. Q. Wang, Y. Y. Sun, B. Lorenz, and C. W. Chu, J. Appl. Phys. **111**, 07D903 (2012).
[9] N. Leo, A. Bergman, A. Cano, N. Poudel, B. Lorenz, M. Fiebig, and D. Meier, Nat. Commun. **6**, 6661 (2015).
[10] I. Urcelay-Olabarria, J. L. García-Muñoz, E. Ressouche, V. Skumryev, V. Yu. Ivanov, A. A. Mukhin, and A. M. Balbashov, Phys. Rev. B **86**, 184412 (2012).
[11] I. Urcelay-Olabarria, J. M. Perez-Mato, J. L. Ribeiro, J. L. García-Muñoz, E. Ressouche, V. Skumryev, and A. A. Mukhin, Phys. Rev. B **87**, 014419 (2013).
[12] I. A. Sergienko and E. Dagotto, Phys. Rev. B **73**, 094434 (2006).
[13] M. Mostovoy, Phys. Rev. Lett. **96**, 067601 (2006).
[14] A. M. Balbashov and S. G. Egorov, J. Cryst. Growth **52**, 498 (1981).
[15] H. Mitamura, S. Mitsuda, S. Kanetsuki, H. A. Katori, T. Sakakibara, and K. Kindo, J. Phys.: Conf. Ser. **51**, 557 (2006).
[16] J. Brown and J. Matthewman, Cambridge Crystallography Subroutine Library Report No. RAL93-009, 1993.
[17] J. Rodriguez-Carvajal, Physica B (Amsterdam) **192**, 55 (1993).
[18] P. J. Becker and P. Coppens, Acta Crystallogr. A **30**, 129 (1974).
[19] The fine details of the structure coming from relativistic interactions are not presented, because they do not provide additional information to understand the evolution of the magnetic structure under magnetic field.
[20] See Supplemental Material at http://link.aps.org/supplemental/10.1103/PhysRevB.96.104435 for agreement plots of the refinements of the magnetic structures under magnetic field applied along the crystallographic b axis.
[21] H. Mitamura, T. Sakakibara, H. Nakamura, T. Kimura, and K. Kindo, J. Phys. Soc. Jpn. **81**, 054705 (2012).
[22] G. Quirion and M. L. Plumer, Phys. Rev. B **87**, 174428 (2013).
[23] N. V. Ter-Oganessian and V. P. Sakhnenko, J. Phys.: Condens. Matter **26**, 036003 (2014).
[24] M. V. Gvozdikova, T. Ziman, and M. E. Zhitomirsky, Phys. Rev. B **94**, 020406(R) (2016).
[25] J. Herrero-Martín, A. N. Dobrynin, C. Mazzoli, P. Steadman, P. Bencok, R. Fan, A. A. Mukhin, V. Skumryev, and J. L. García-Muñoz, Phys. Rev. B **91**, 220403(R) (2015).
[26] E. V. Sinitsyn and I. G. Bostrem, Zh. Eksp. Teor. Fiz. **85**, 661 (1983) [Sov. Phys. JETP **58**, 385 (1983)].
[27] V. N. Milov, G. G. Artem'ev, V. I. Nedel'ko, A. F. Prun, M. V. Semenova, and E. V. Sinitsyn, Zh. Eksp. Teor. Fiz. **88**, 272 (1985) [Sov. Phys. JETP **61**, 159 (1985)].